Available online at www.sciencedirect.com

ScienceDirect

Journal of Taibah University for Science 11 (2017) 654–660

Journal of Taibah University for Science

www.elsevier.com/locate/jtusci

Resistivity–thermopower correlation derived temperature-dependent transport behaviour of $Mn_xZn_{1-x}Fe_2O_4$ nanoparticles

Jaison Joseph [a,*], R.B. Tangsali [b], S.M. Gurav [c]

[a] *Department of Physics, Govt. College, Khandola, Goa 403107, India*
[b] *Department of Physics, Goa University, Taleigao Plateau, Goa 403206, India*
[c] *Department of Chemistry, Govt. College, Quepem, Goa 403705, India*

Received 4 December 2015; received in revised form 1 September 2016; accepted 6 September 2016
Available online 26 September 2016

Abstract

Ferrite material nanoparticles comprised of manganese and zinc were chemically synthesized by the co-precipitation method. The designated ferrite X-ray diffraction peaks and characteristic ferrite absorption bands in Fourier transform infrared absorption spectra confirmed the formation of a spinel structure. Determination of the full width at half maximum values of the X-ray diffraction peaks and the corresponding calculations using the Scherrer formula suggested the generation of nano-grains. Micrographs obtained using a transmission electron microscope confirmed the nano-scale dimensions of the particles. Deviations in the characteristic resistivity and thermopower values in response to ambient sample temperature variations were experimentally observed and used for correlation-derived temperature-dependent transport behaviour analysis. Samples with a concentration $x = 0.8$ and 1.0 showed high thermopower values at reasonably low temperatures with moderate specific resistance.

Keywords: Ferrite nanoparticles; Resistivity; Thermopower; Transport behaviour analysis; Spin-Seebeck effect

1. Introduction

A significantly high deviation of the physical properties of materials at nano-scale dimensions aroused curiosity and renewed interest in many already familiar materials in the broad domain of industrially feasible materials. Spinal ferrites can be classified as belonging to these materials because of their commercial importance in industry that utilise a combination of excellent electrical and soft magnetic properties. The co-existence of high relative magnetic and electric polarization along with high electrical resistivity observed in spinel ferrite materials has led to the abundant use of this material in the electronics industry. Mixed spinel ferrites, essentially with low hysteresis loss and small particle sizes, are considered to be emerging materials for novel applications in areas such as drug delivery systems and hyperthermia [1]. Manganese zinc (Mn–Zn) spinel ferrite, which can be produced at a practical cost, is extensively used in a large number of electronic devices that utilize its favourable physical properties, such as high permeability at high frequency, remarkably high electrical resistivity, good mechanical hardness,

* Corresponding author.
E-mail address: jaisonjosephp@gmail.com (J. Joseph).
Peer review under responsibility of Taibah University.

Production and hosting by Elsevier

http://dx.doi.org/10.1016/j.jtusci.2016.09.005

and reasonable chemical stability. A recent research study conducted on Mn–Zn ferrite materials fabricated in nano-scale thin films revealed an enhancement of the magnetic property of coercivity [2–5]. Investigations conducted using the Mössbauer spectroscopy technique to probe the structural and magnetic property deviations in gamma irradiated Mn–Zn nanoferrite materials revealed amazing alterations in the cation distribution [6]. An enhancement of the industry-oriented useful properties of Mn–Zn ferrite materials through the modification of the cation distribution inside the nanoparticles by exposing it to gamma radiation was reported recently [7]. In another study, the introduction of Al^{3+} ions into Mn–Zn nano ferrite materials was found to increase its resistivity at a lower temperature range [8].

The experimentally observed transport properties in ferrites, specifically resistivity and thermopower, provide valuable information regarding the behaviour of localized electric charge carriers, leading to the greater understanding of the transport mechanism. Further, thermoelectric power generation is an emerging technology that may be the solution to current environmental and energy issues around the world [9]. This type of power generation is primarily based on electric conductors that show substantial generation of electric voltage over a reasonable difference in temperature caused by the Seebeck effect. However, the present constraints of efficiency and device costs place a reasonable restriction on the use of thermoelectric power generation based on this effect. The recently discovered spin-Seebeck effect (SSE) [10], which involves the generation of spin voltage, has the potential to drive a non-equilibrium spin current [11] from a heat current in magnetic metals, semiconductors and magnetic insulators, thereby providing a method of overcoming the abovementioned constraints by making use of insulators as thermoelectric power sources. Using a suitable coupling of a paramagnetic metal to a magnetic insulator, the thermally generated spin voltage can be converted into electrical voltage via the inverse spin-Hall effect (ISHE) [12]. By identifying an insulator with low thermal conductivity to suppress energy loss caused by heat conduction, the use of SSE could enhance the thermoelectric power generation efficiency [13]. A recent report highlighted the appearance of the longitudinal spin-Seebeck effect in a sintered polycrystalline bulk (Mn–Zn)Fe_2O_4 slab [14]. The effect drives a spin current to flow across an interface between the (Mn–Zn)Fe_2O_4 slab and an attached Pt film along a temperature gradient to generate an electric voltage via the inverse spin-Hall effect in the Pt film. Because this observed phenomenon enables thermal generation of an electric voltage from a commonly used polycrystalline insulator, it has the potential to be used as a versatile and low-cost thermoelectric power generator. This paper aims to identify an appropriate stoichiometric composition of a Mn–Zn ferrite thermoelectric material based on the resistivity–thermopower correlation derived temperature-dependent transport behaviour analysis of $Mn_xZn_{1-x}Fe_2O_4$ nanoparticles for probable utilization in the manufacturing of devices based on the spin-Seebeck effect.

2. Experimental

Nanoparticles of $Mn_xZn_{1-x}Fe_2O_4$ ($x = 0.0$, 0.2, 0.4, 0.6, 0.8 and 1.0), wherein x represents the stoichiometric concentration index, were prepared by co-precipitating aqueous solutions of $ZnSO_4$, $MnCl_2$ and $FeCl_3$ mixtures in an alkaline medium [15]. The base materials $ZnSO_4{:}7H_2O$, $MnCl_2{:}6H_2O$ and $FeCl_3{:}6H_2O$ were taken in their respective stoichiometry, dissolved in distilled water, and then heated to 65 °C. The respective metal ions were precipitated by adding a suitable precipitating reagent while boiling the solution for 10 s under constant stirring. After maintaining the solution along with the precipitate at 80 °C for 1 h, the precipitate was filtered and dried at 100 °C. The dried powder was pelleted and subjected to heat treatment in a box furnace at the desired temperature and temperature ramp rate for 15 h, resulting in the formation of $Mn_xZn_{1-x}Fe_2O_4$ nanoparticles.

The powdered samples were characterized using a high-intensity rotating anode Rigaku X-ray diffractometer. The Fourier transform infrared (FT-IR) absorption spectra of the samples were recorded on a Shimadzu 8900 FT-IR spectrometer. Transmission electron microscope (TEM) micrographs were taken on a Hitachi-H-7650. The resistivity measurements were performed via the two probe method using a Keithley electrometer (model 6514) by maintaining a constant voltage across the sample. Thermo-electric power (TEP) measurements were conducted on an automated indigenously built, laboratory based set-up at temperatures ranging from 0 °C to 200 °C.

3. Results and discussion

The X-ray diffraction (XRD) pattern for $Mn_xZn_{1-x}Fe_2O_4$ is shown in Fig. 1.

The positions of the observed intensity peaks, which are in agreement with the reported and established ferrite peak positions derived by Rietveld refinement [6], confirm the formation of a single phase cubic spinel

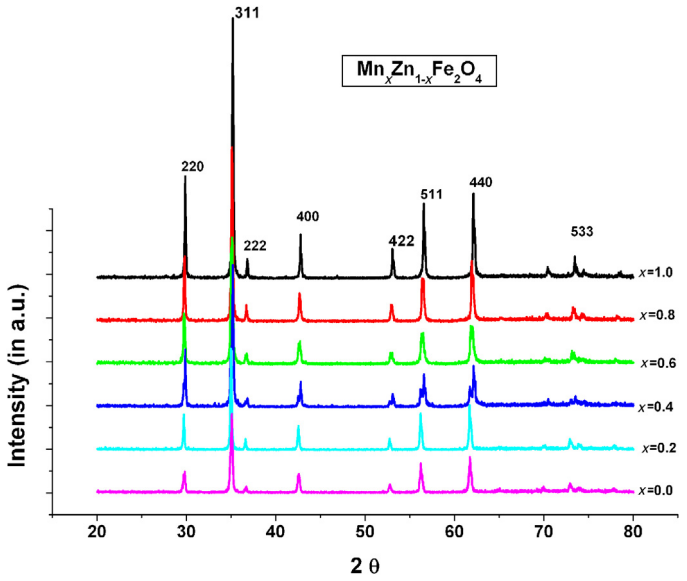

Fig. 1. XRD pattern of $Mn_xZn_{1-x}Fe_2O_4$.

structure. The crystal interplanar spacing (d) was calculated using Bragg's law, presented as Eq. (1).

$$2d \sin\theta = n\lambda \tag{1}$$

where θ represents the angle of incidence, n is an integer and λ is the wavelength of the X-ray source used for diffraction studies. The value of lattice constant 'a' was obtained by substituting the corresponding 'd' values in Eq. (2) given below.

$$a = d\sqrt{h^2 + k^2 + l^2} \tag{2}$$

where h, k and l are the Miller indices.

The calculated numerical values for the grain size were obtained by substitution of the full width at half maximum values (β) in the Debye Scherrer formula (Eq. (3)) given below.

$$D = \frac{0.9\lambda}{\beta \cos\theta} \tag{3}$$

The numerical values of the lattice constant and the grain size were calculated for each spinel peak position in the XRD data; the average values for the samples are listed in Table 1.

The variation of the lattice constant and grain size with respect to the increase in Mn concentration along with the estimated error presented in Table 1 is reproduced in Fig. 2a and b.

The lattice constant 'a' (8.4615 Å) for $x = 0.0$ with a consistent gradual increase up to 8.5078 Å for $x = 1.0$ due to the substitution of Mn^{2+} ions with a larger radius (0.8 Å) in place of Zn^{2+} ions with a smaller radius (0.74 Å), is in good agreement with numerous literature reports [6,16–18]. The dependence of the particle size with respect to the Mn concentration does not show any specific trend, and the average particle size is found to be 44 nm.

Table 1
Variation of lattice constant and particle size.

Mn concentration x	Lattice constant 'a' in Å	Particle size D in nm
0.0	8.4615 ± 004	47 ± 2
0.2	8.4621 ± 002	41 ± 2
0.4	8.4748 ± 005	36 ± 1
0.6	8.4847 ± 004	46 ± 2
0.8	8.4848 ± 006	34 ± 2
1.0	8.5078 ± 005	40 ± 3

The IR absorption spectra show two broad absorption bands, as shown in Fig. 3. The higher band ν_1 between 610–550 cm^{-1} and lower band ν_2 between 450–375 cm^{-1}, which are expected common features for ferrites, are prominently observed in all samples. It is observed that the Me_T–Me_O stretching vibration at 350–330 cm^{-1} is weak and merges with the Me_O–O stretching vibration at 450–485 cm^{-1}, forming the single wide band ν_2. The observed band ν_1 is due to Me_T–O–Me_O stretching vibrations. Me_O represents the metal in octahedral sites, Me_T represents the metal in tetrahedral sites and O represents oxygen. This reveals the formation of a single phase spinel structure with two sub lattices [19].

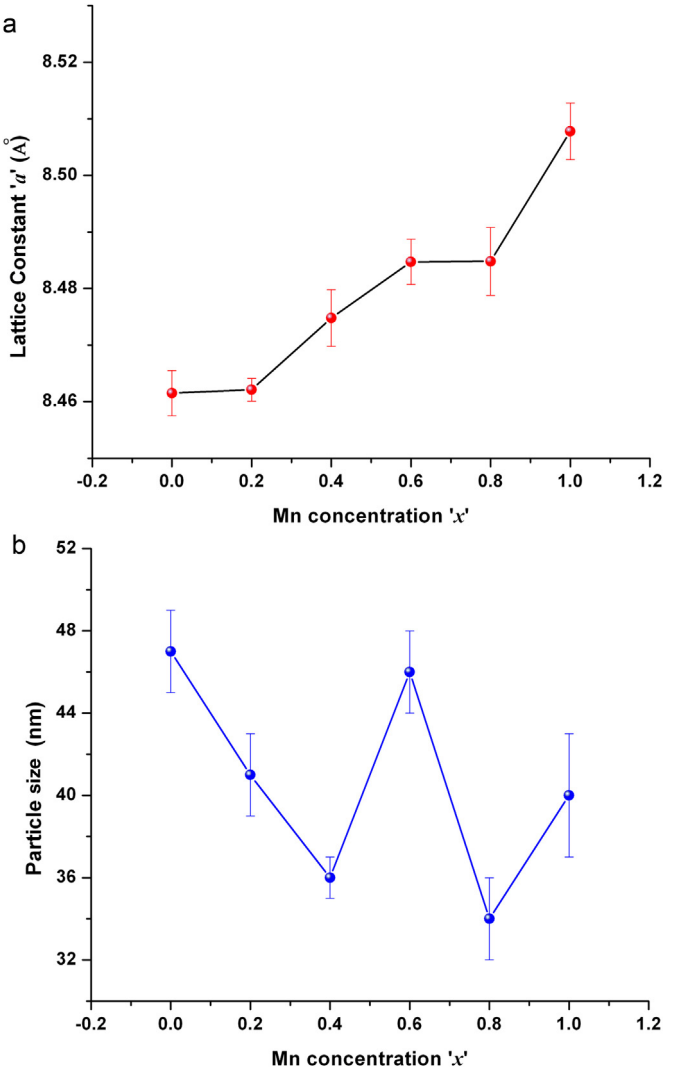

Fig. 2. Variation of the lattice constant and grain size.

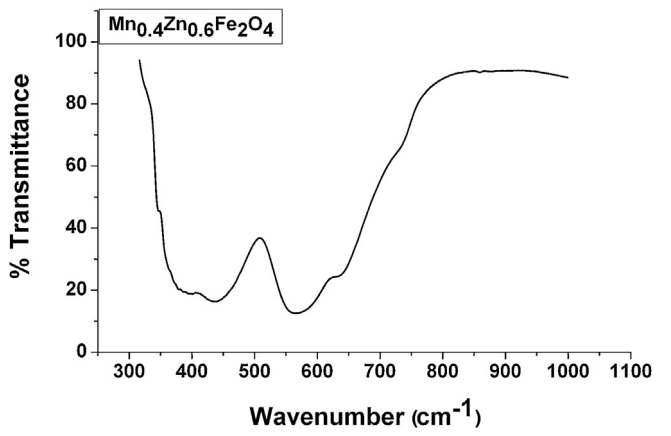

Fig. 3. FT-IR spectra of $Mn_xZn_{1-x}Fe_2O_4$.

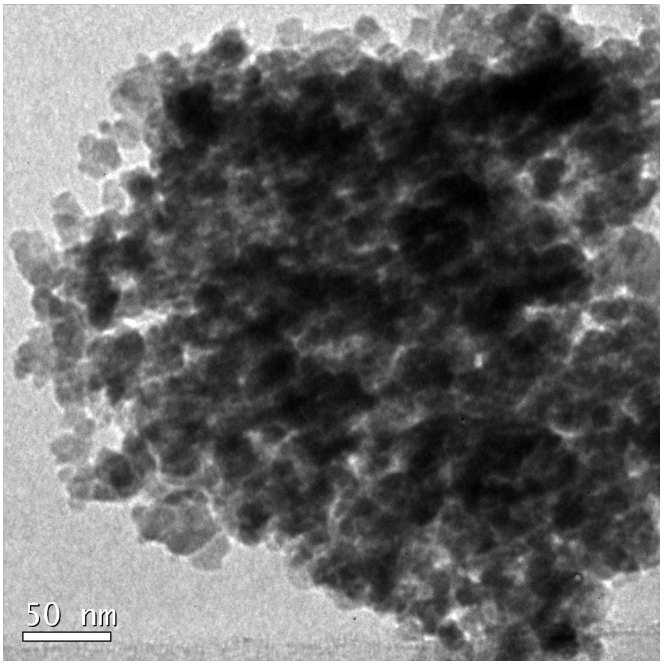

Fig. 4. TEM monograph of $Mn_{0.6}Zn_{0.4}Fe_2O_4$.

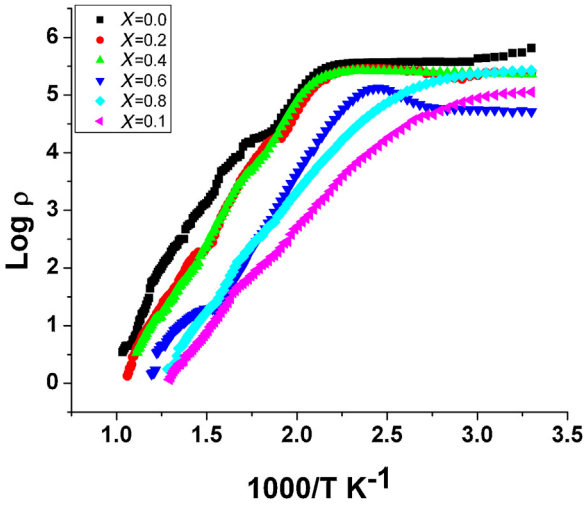

Fig. 5. DC resistivity of $Mn_xZn_{1-x}Fe_2O_4$.

The particle sizes and morphologies of the samples were investigated using TEM micrographs. Analysis of the micrographs (see Fig. 4) revealed a near spherical shape of the nanoparticles with reasonably low agglomeration. The sizes of the particles appearing in the TEM micrograph were found to be consistent with the grain sizes determined from the XRD data.

The temperature-dependent dc resistivity measured from room temperature to 550 °C is shown in Fig. 5. For all samples, the variation of resistivity with increasing temperature is found to follow a trend that is indicative of semiconductive behaviour, which could be described as the Arrhenius relation presented in Eq. (4):

$$\rho = \rho_0 \exp - \left(\frac{E}{KT}\right) \tag{4}$$

where E is the activation energy, K is the Boltzmann constant, T is temperature and ρ_0 is a temperature-independent constant.

The prominent change in slope indicates that a change in the conduction mechanism occurred over the temperature range of 353–478 K for all samples. This change in slope was found to be predominantly sharp for samples up to $x = 0.6$ and relatively gradual for samples $x = 0.8$ and 1.0. A mild slope change indicative of a shift in conduction behaviour was observed at 533 K, 593 K, 638 K, 728 K, and 838 K for sample $x = 0.0$. This trend was repeated for samples $x = 0.2$, 0.4 and 0.6. For sample $x = 0.8$, this mild slope change was observed in four steps at temperatures of 533 K, 603 K, 633 K and 738 K; the number of steps was found to be reduced to three at temperatures of 508 K, 608 K and 723 K for sample $x = 1.0$.

In general, for ferrites, the first low-temperature region (up to approximately 423 K) is attributed to the effects of conduction on the surface-absorbed impurities, including moisture, voids and defects. The second temperature region (up to the Curie temperature) is

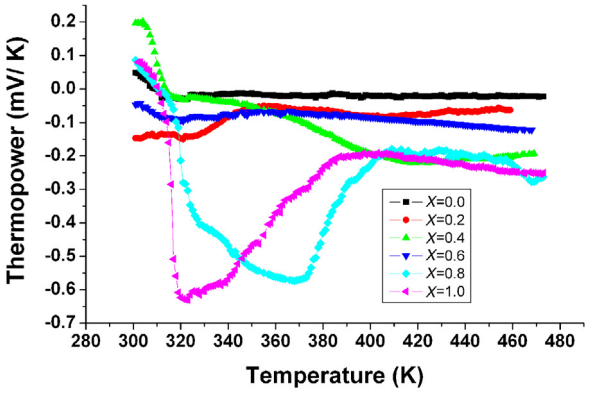

Fig. 6. Variation of thermopower with temperature.

the ferrimagnetic region. The third temperature region (above the Curie temperature) is the paramagnetic region [20].

Thermo-electric power (TEP) measurements conducted on the samples are presented in Fig. 6. TEP analysis confirmed the semiconducting nature of the material, with a predominance of n-type charge carriers for all samples. At room temperature, p-type conduction was observed for samples $x = 0.0$, 0.4, 0.8 and 1.0, which shifted to n-type conduction well before 320 K. However, for the samples with $x = 0.2$ and 0.6, the n-type charge concentration was predominant, with reasonable amplitude fluctuations. A maximum thermopower value of -0.629 mV/K was observed for sample $x = 1.0$ at 320 K, followed by -0.574 mV/K for sample $x = 0.8$ at 370 K.

Because $Mn_xZn_{1-x}Fe_2O_4$ nanoparticles with concentrations of $x = 0.8$ and 1.0 showed sensible thermopower values at reasonably lower temperatures, the resistivity–thermopower correlation derived temperature-dependent transport behaviour of these samples was the focus of this study; a visual representation of this behaviour in graphical form is shown in Figs. 7 and 8. The samples experienced a moderate specific resistance of 100 kΩ and 140 kΩ at temperatures in which the maximum thermopower was observed. Thus, samples with a concentration of $x = 1.0$ showed a maximum thermopower value at a lower temperature with a slightly higher specific resistance compared to those of the samples with a concentration = 0.8.

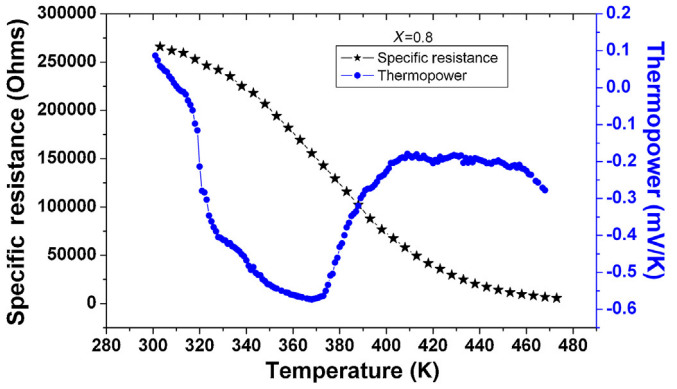

Fig. 7. Variation of thermopower and specific resistance with temperature ($x = 0.8$).

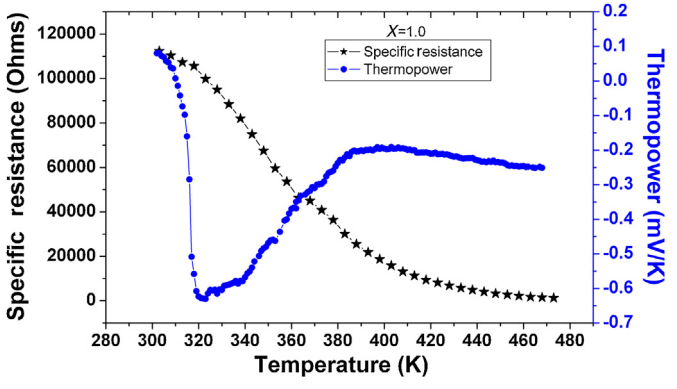

Fig. 8. Variation of thermopower and specific resistance with temperature ($x = 1.0$).

4. Conclusions

Polycrystalline ferrite nanoparticles of $Mn_xZn_{1-x}Fe_2O_4$ ($x = 0.0$, 0.2 0.4, 0.6, 0.8 and 1.0) were prepared via the co-precipitation method. The samples were characterized using XRD and FT-IR spectroscopy. The dimensions of the crystalline grain sizes estimated from the XRD data were corroborated by the particle sizes observed in TEM micrographs. Conductivity and thermopower measurements of the samples were performed on pelleted material; and then, the resistivity–thermopower correlation derived temperature-dependent transport behaviour of $Mn_xZn_{1-x}Fe_2O_4$ nanoparticles with concentrations of $x = 0.8$ and 1.0 was analysed. Nano-scale ferrite samples with a concentration of $x = 1.0$ were found to exhibit the maximum thermopower value at a lower temperature with a slightly higher specific resistance compared to those of samples with a concentration of $x = 0.8$. This analysis highlights the suitability of $Mn_xZn_{1-x}Fe_2O_4$ nanoparticles with a stoichiometry of $x = 0.8$ and 1.0 as preferred material for use in emerging thermoelectric power generation applications involving the longitudinal spin-Seebeck effect.

Acknowledgment

This work is supported by the University Grants Commission, Govt. of India, under research project UGC/47-820/04 (WRO).

References

[1] M.P. Marszall, Pharm. Res. 28 (3) (2011) 480–483.
[2] J. Joseph, R.B. Tangsali, V.P. Mahadevan Pillai, R.J. Choudhary, D.M. Phase, V. Ganeshan, Adv. Sci. Lett. 22 (2016) 825–829.
[3] J. Joseph, R.B. Tangsali, V.P. Mahadevan Pillai, R.J. Choudhary, D.M. Phase, V. Ganeshan, Physica B 456 (2015) 293–297.
[4] J. Joseph, R.B. Tangsali, V.P. Mahadevan Pillai, R.J. Choudhary, D.M. Phase, V. Ganeshan, Mater. Res. Bull. 61 (2014) 475–480.
[5] J. Joseph, R.B. Tangsali, R.J. Choudhary, D.M. Phase, V. Ganeshan, Int. J. Thin Films Sci. Technol. 3 (2014) 81–87.
[6] P.P. Naik, R.B. Tangsali, S.S. Meena, P. Bhatt, B. Sonaye, S. Sugur, Radiat. Phys. Chem. 102 (2014) 147–152.
[7] P.P. Naik, R.B. Tangsali, B. Sonaye, S. Sugur, J. Magn. Magn. Mater. 385 (2015) 377–385.
[8] S.J. Haralkar, R.H. Kadam, S.S. More, S.E. Shirsath, M.L. Mane, S. Patil, D.R. Mane, Mater. Res. Bull. 48 (2013) 1189–1196.
[9] F.J. DiSalvo, Science 285 (1999) 703–706.
[10] J. Xiao, G.E.W. Bauer, K. Uchida, E. Saitoh, S. Maekawa, Phys. Rev. B 81 (2010) 214418.
[11] S. Maekawa, Concepts in Spin Electronics, Oxford University Press, 2006.
[12] O. Mosendz, J.E. Pearson, F.Y. Fradin, G.E.W. Bauer, S.D. Bader, A. Hoffmann, Phys. Rev. Lett. 104 (2010) 046601.
[13] K. Uchida, J. Xiao, H. Adachi, J. Ohe, S. Takahashi, J. Ieda, T. Ota, Y. Kajiwara, H. Umezawa, H. Kawai, G.E.W. Bauer, S. Maekawa, E. Saitoh, Nat. Mater. 9 (2010) 894–897.
[14] K.-i. Uchida, T. Nonaka, T. Ota, E. Saitoh, Appl. Phys. Lett. 97 (2010) 262504.
[15] J. Joseph, R.B. Tangsali, S.M. Gurav, IOP Conf. Series: Materials Science and Engineering, vol. 73, 2015, p. 012098.
[16] W.H. Kwon, J.-G. Lee, S.W. Lee, K.P. Chae, J. Korean Phys. Soc. 57 (2010) 1965–1969.
[17] X. Hou, J. Feng, X. Liu, Y. Ren, Z. Fan, M. Zhang, J. Colloid Interface Sci. 353 (2011) 524–529;
R.B. Tangsali, S.H. Keluskar, G.K. Naik, J.S. Budkuley, Int. J. Nanosci. 3 (2004) 589–597.
[18] S.G. Dahotre, L.N. Singh, Arch. Phys. Res. 2 (1) (2011) 81–89.
[19] P.P. Naik, R.B. Tangsali, B. Sonaye, S. Sugur, AIP Conf. Proc. 1512 (2013) 354–355.
[20] R.B. Tangsali, S.H. Keluskar, G.K. Naik, J.S. Budkuley, J. Mater. Sci. 42 (2007) 878–882.